

First principles investigation of epitaxially strained ATiO₃/TiO (A=Sn,Pb) superlattice

S. Raza,¹ R. Zhang,² N. Zhang,³ Z. Li,⁴ L. Liu,⁵ F. Zhang,¹ D. Wang,^{1,*} and C.-L. Jia^{1,6}

¹*School of Microelectronics & State Key Laboratory for Mechanical Behavior of Materials,*

Xi'an Jiaotong University, Xi'an 710049, China

²*School of Engineering and Materials Science,*

Queen Mary University of London, London E1 4NS, United Kingdom

³*Electronic Materials Research Laboratory–Key Laboratory of the Ministry of Education and International Center for Dielectric Research,*

Xi'an Jiaotong University, Xi'an 710049, China

⁴*School of Materials Science and Engineering,*

University of Science and Technology Beijing, Beijing 100083, China

⁵*College of Materials Science and Engineering,*

Guilin University of Technology, Guilin, 541004, China

⁶*Ernst Ruska Center for Microscopy and Spectroscopy with Electrons,*

Research Center Jülich, D-52425 Jülich, Germany

(Dated: July 17, 2019)

Abstract

Combining layers of different materials to form superlattice is one way to engineer novel material structures with enhanced properties. Here, we propose a superlattice made of ATiO₃ (A=Sn,Pb) and TiO layers with the general formula A_nTi_{4n}O_{7n}. First principles results show that such structures can have significant polarization owing to their intrinsic structure due to the huge lattice mismatch between the two types of layers. Different ferroelectric phases of the superlattice, which are based on a number of polymorphs of the perovskite ATiO₃ (e.g. *P4/mmm, P4mm, Amm2, Pmm2, Pm,* and *Cm*), are investigated under epitaxial strain to explore their energy and polarization dependence on different substrates. The results indicate stable existence of the ferroelectric *Cm* and *Amm2* phases for a wide range of strains.

I. INTRODUCTION

The structure of a crystal is one of the most important factor that determine its properties. For ferroelectric and piezoelectric materials, strain engineering has been widely used to their performances^{1,2-3}. In fact, ferroelectric materials owe their technological significance to their ability of retaining switchable polarization, which can be tuned with epitaxial strain and electric field⁵. The effects of misfit strain on structural properties and polarization have been studied extensively in the past both theoretically and experimentally⁶⁻⁸.

Researches have also proposed other crystal structures, which is a combination of perovskite and other oxides, to go beyond perovskites and achieve better performance. One combination of perovskites with their own constituent oxides is known as Ruddlesden Popper (RP) phase where a single rocksalt layer oxide (AO) is added (with some in-plane shift) between AO terminated n layers of perovskite ABO_3 slabs ($n = 1, 2, 3 \dots$), resulting in the general formula of $A_{n+1}B_nO_{3n+1}$ ^{12,13} [see Fig. 1(b)], whose ferroelectric nature has been thoroughly investigated for Sn_2TiO_4 and Pb_2TiO_4 ^{26,28}.

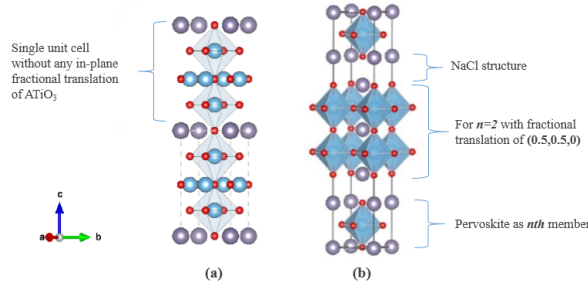


Figure 1. (a) $1 \times 1 \times 2$ superlattice model of $A_nTi_{4n}O_{7n}$ (A=Sn) grown along the z -direction. (b) Crystal structure of $A_{n+1}Ti_nO_{3n+1}$ (A=Sn)- RP phase. The grey spheres represent Sn atoms while blue and red speheres represent Ti and O atoms respectively.

Interestingly, there exists another possibility is to consider adding BO layers. For $ATiO_3$ system, this means adding TO layers. This possibility is largely ignored since the misfit strain between $ATiO_3$ and TiO could be huge. Nonetheless, given the recent discovery of giant polarization in high lattice mismatch crystal structures where the perovskite undergoing a huge 16.5% tensile strain, it becomes clear that the $ATiO_3/TiO$ possibility needs to be explored²³. While many possibilities for perovskites junctioned with TiO_2 have been explored to optimize their photoelec-

trochemical and photocatalytic properties²⁵, the use of TiO for stabilize (or enhance) the ferroelectricity of perovskites lacks any prior investigation. The general formula for such superlattice is $A_n\text{Ti}_{4n}\text{O}_{7n}$ ($n = 1, 2, 3 \dots$), different from the RP structure ($A_{n+1}\text{Ti}_n\text{O}_{3n+1}$) as shown in Fig.1, which likely making them a new class of materials.

In this work, we will investigate the superlattices made of ATiO_3/TiO ($A=\text{Sn,Pb}$) with and without epitaxial strain. The in-plane lattice mismatch between ATiO_3 and TiO is potentially beneficial for inducing large polarization (the in-plane lattice parameter of TiO is considerably larger than its perovskite counterpart).

Practically, cubic perovskite ATiO_3 and rocksalt TiO are combined to form the superlattices, which is assumed to be grown along the z -axis as shown in Fig. 1 (a). The superlattice is essentially a repetition of the unit cell containing 12 atoms: $\text{AO-TiO}_2\text{-2TiO-TiO}_2$ ($A=\text{Sn,Pb}$) [atoms in Fig. 1 (a) enclosed by the dotted lines], noting that the TiO layer has two Ti atoms and two O atoms in one unit cell. In such a configuration, both the TiO layer and the ATiO_3 layer experience strains due to their lattice mismatch. We also consider such superlattice epitaxially grown on different substrates, subjecting to misfit strains. With the aid of well-known ferroelectric perovskite phases, we carry out first-principles calculations for a few structural phases, which shows that the monoclinic Cm phase is stable for a wide range of compressive strain, which highlights the ease of stabilizing the monoclinic phase with $A_n\text{Ti}_{4n}\text{O}_{7n}$ superlattices¹⁴⁻¹⁶ and demonstrates TiO is instrumental to forming and stabilizing novel ferroelectric oxides.

This paper is organized as the follows. In Sec. II, we show details regarding our *ab initio* computation used in this work. In Sec. III, we investigate the possible phases appearing in such compounds, whose polarizations are obtained in Sec. III B. The structures of this new class of materials is further discussed in Sec. III. Finally, we give a brief conclusion in Sec. IV.

II. METHOD

The structures of the proposed superlattices are fully relaxed using the projector augmented plane wave (PAW) method as implemented in the GPAW Package¹⁸. The localized density approximation (LDA) is used with a cut-off energy of 750 eV to ensure the convergence. A $4 \times 4 \times 2$ Monkhorst-Pack²⁷ sampling is used for the k -space integration. The valence orbitals used in the first-principles calculations are: Pb ($6s\ 6p\ 5d$), Ti ($3s\ 3p\ 4s\ 3d$) and O ($2s\ 2p$). The atomic positions and lattice constants are relaxed until both atomic forces and stresses fall below $0.005\ \text{V}/\text{\AA}$.

This process will provide us with the energy and structural information of the SL at a given symmetry, i.e., $P4/mmm$, $P4mm$, Pm , $Amm2$, $Pmm2$, and Cm . The electric polarizations for different phases of each structure are calculated using the Berry Phase method as implemented in ABINIT software package¹⁹. All the crystal structures under consideration are created using Atomic Simulation Environment and visualized with VESTA¹⁷. To be certain that the relaxation procedure is correct, we have used the same setup and calculated lattice parameters and spontaneous polarization of SnTiO_3 and PbTiO_3 , which agree well with previous results (see App. A).

For geometry optimization, we set up the initial configurations of the superlattice by distorting the titanium atoms in the perovskite structure along high-symmetry directions to form the $P4/mmm$, $P4mm$, Pm , $Amm2$, $Pmm2$, and Cm phases⁵. The overall symmetry of our superlattice is considered both before and after relaxation. In addition, we replicate the biaxial strain effect on the superlattices by fixing their in-plane lattice constant while optimizing the atom positions and the out-of-plane lattice constant. The misfit strain is calculated as $\epsilon = (a - a_0)/a_0$ where a_0 is the LDA optimized lattice constant of the superlattice without the in-plane constraint²². The equivalent atomic forces of the stress tensor components are optimized to fall below 0.005 eV/\AA .

III. RESULTS AND DISCUSSION

The initial lattice constants of SnTiO_3 and PbTiO_3 with ions in ideal positions ($P4/mmm$ symmetry) have the lattice constant of $a = 3.79$, $c = 4.175 \text{ \AA}$ ²⁹, and $a = 3.89$, $c = 4.15 \text{ \AA}$ ²³, respectively. On the other hand, the rocksalt TiO has a lattice constant of 4.17 \AA ³⁰ with the $Fm\bar{3}m$ symmetry. We can clearly anticipate the stretching of perovskite part in the x - y plane when it is grown with TiO. In this section, we perform two sets of calculations to investigate (i) the most stable structure of ATiO_3/TiO ($A=\text{Sn,Pb}$) superlattice without subjecting to any misfit strain and (ii) How the structural phases of ATiO_3/TiO ($A=\text{Sn,Pb}$) superlattice evolve with epitaxial strain assuming (i.e. if the ATiO_3/TiO superlattice is grown on some substrates.

A. Structural phases

When we stack ATiO_3 layers with TiO layers, it is equivalent to replacing every second AO layer with the TiO layer, which results in the $P4/mmm$ symmetry if the original cubic perovskite cells are not distorted. In addition to the $P4/mmm$ symmetry, we also set the perovskite part to

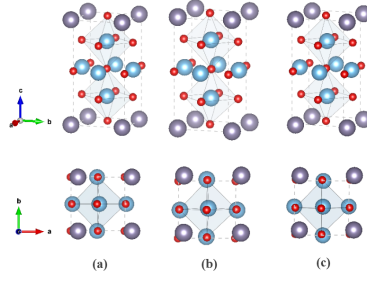


Figure 2. Different phases of the $\text{SnTiO}_3\text{-TiO}$ superlattice after structural relaxation: (a) Pm (b) Cm (c) $Amm2$. The figures in the first and second rows are views from different angles.

some well known phases (i.e., $P4mm$, Cm , $Amm2$, $Pmm2$, and Pm phases), which are then used as the initial configuration to relax the superlattice. Hereafter, we will base our calculations on these six phases. The relaxed ATiO_3/TiO ($A=\text{Sn,Pb}$) structures for the Cm and $Amm2$ phases are shown in Fig.2 which shows a large displacement of atoms in the $x - y$ plane with a relatively smaller shift in the z direction. Table II states the atomic displacements for the Pm , Cm , and $Amm2$ phases of ATi_4O_7 while basic propertise of the relaxed structures are stated in Tab. I, which shows that SnTi_4O_7 and PbTi_4O_7 has the Cm phase and the $Amm2$ phase, respectively, as the ground state.

Moreover, Tab. II shows ion displacements (in fractional coordinates) of ATi_4O_7 where SnTi_4O_7 has larger ion shifts in both the Cm and the $Amm2$ phases than PbTi_4O_7 . In particular, the Sn has a 10 times larger displacement than Pb due to its smaller size, indicating a larger polarization (see Tab. 5).

For the relaxed ATi_4O_7 , the perovskite part SnTiO_3 (PbTiO_3) experiences a tensile strain of about 3.96% (3.80%) while the TiO undergoes a compression of about 4% for each of the two cases [$a_o = 3.86$ (SnTiO_3), $a_o = 3.87$ (PbTiO_3), $a_o = 4.18$ (TiO)]^{22,26}. The tensile strain forces the ATiO_3 component into a pseudocubic structure ($a = b = 4.01 \text{ \AA}$ and $c/2 = 3.95 \text{ \AA}$). The ground state in-plane lattice constants for SnTi_4O_7 and PbTi_4O_7 are almost the same, which can be attributed to the rigid nature of TO layer to restrict any of its further compression. For the relaxed structures, except for the $P4mm$ and the $P4/mmm$ phases, all the other phases have close energies, indicating that (i) ion displacement along the z direction is suppressed and (ii) the ions have more room to shift inside the x - y plane.

Since it is a common practice to grow superlattices on different substrates to engineer epitaxial strain, in order to understand how the ATiO_3/TiO superlattice behaves when they are grown on

Property	$a(\text{\AA})$	$b(\text{\AA})$	$c(\text{\AA})$	α	β	γ	Energy	
SnTi ₄ O ₇	<i>P4/mmm</i>	4.0067	4.0067	7.8791	90	90	90	-108.4859
	<i>P4mm</i>	4.0069	4.0069	7.9261	90	90	90	-108.5021
	<i>Pmm2</i>	4.0116	4.0117	7.9178	90	90	90	-108.6356
	<i>Amm2</i>	4.015	4.015	7.9039	90	90	89.33	-108.6361
	<i>Pm</i>	4.011	4.012	7.9193	90	89.98	90	-108.6357
	<i>Cm</i>	4.013	4.013	7.9125	89.98	89.98	89.54	-108.6585
PbTi ₄ O ₇	<i>P4/mmm</i>	4.012	4.012	7.8964	90	90	90	-108.7942
	<i>P4mm</i>	4.013	4.013	7.8974	90	90	90	-108.7943
	<i>Pmm2</i>	4.023	4.000	7.8946	90	90	90	-108.8260
	<i>Amm2</i>	4.012	4.012	7.8950	90	90	89.88	-108.8316
	<i>Pm</i>	4.023	4.000	7.8957	90	89.99	90	-108.8262
	<i>Cm</i>	4.012	4.012	7.8946	89.98	89.98	89.87	-108.8315

Table I. Properties of different phases of ATiO₃-TiO (A=Sn,Pb) superlattice after relaxation. The rocksalt TiO has a lattice constant of 4.177 Å. Energy is eV per formula.

substrates, we have put them under epitaxial strain and obtained the energies of the aforementioned phases, which are shown in Fig. 3. Since the *P4mm* and *P4/mmm* phases have a much larger energy than the other phases over the whole strain range, they are omitted from Fig. 3. The rest of the four phases (i.e. *Pm*, *Pmm2*, *Cm*, and *Amm2*) have very close energies as seen in Fig. 3.

Figure 3(a) shows that SnTi₄O₇ has the *Cm* phase as the ground state for a wide range of mistfit strain until $a = 4.10 \text{ \AA}$ ($\approx 2.15\%$ tensile strain) when the *Amm2* phase becomes most stable because the in-plane shift becomes more important at this point. Figure 3(b) shows a similar behavior for PbTi₄O₇ where the *Cm* phase is most stable until $a = 4.05 \text{ \AA}$ ($\approx 0.95\%$ tensile strain), after which, the *Amm2* phase starts to dominate the resulting system. Interestingly, over the whole misfit strain range, while the *Pm* [with polarization direction $(u, 0, w)$] and *Pmm2* $[(u, 0, 0)]$ phases are very close in energy to the *Amm2* $[(u, u, 0)]$ and the *Cm* $[(u, u, w)]$ phases, while their polarization directions differ.

Figure4 shows that the $(c/2)/a$ ratio of ATi₄O₇ (A=Sn,Pb), which can be compared with the c/a ratio of ATiO₃, decreases with an increasing in-plane lattice constant. Over the whole misfit strain range, the $(c/2)/a$ ratio of SnTi₄O₇ remains higher than PbTi₄O₇, which is likely due to

Structure	Atoms	SnTi ₄ O ₇			PbTi ₄ O ₇		
		<i>Cm</i>		<i>Amm2</i>	<i>Cm</i>		<i>Amm2</i>
		Δx	Δz	Δx	Δx	Δz	Δx
ATiO ₃	A	0.096	0.016	0.096	0.010	0.015	0.010
	Ti	0.023	0.004	0.025	0.018	0.001	0.018
	O	-0.006	0.015	-0.007	0.019	0.015	0.019
	O	0.016	0.008	0.015	0.018	0.007	0.018
	O	0.002	0.008	0.006	0.021	0.007	0.021
TiO	Ti	-0.008	0.015	0.028	0.037	0.015	0.037
	Ti	0.028	0.015	-0.002	0.004	0.015	0.004
	O	-0.001	0.014	0.021	0.030	0.015	0.030
	O	0.030	0.015	-0.003	0.003	0.015	0.002
TiO ₂	Ti	0.023	0.026	0.025	0.018	0.028	0.018
	O	0.002	0.021	0.005	0.021	0.022	0.021
	O	0.016	0.021	0.015	0.018	0.022	0.018

Table II. Displacement of atoms (in reduced coordinates) with respect to their ideal positions in *Cm* and *Amm2* phase ATi₄O₇ (A=Sn,Pb). Δx and Δz represent displacements along the x and z directions, respectively. Note that both the *Cm* and the *Amm2* phases have $\Delta x = \Delta y$, while the *Amm2* phase further has $\Delta z = 0$.

the higher tetragonality of the parent SnTiO₃(1.13)²² as compared to that of PbTiO₃(1.065)³². As we know, at 3.85 Å epitaxially strained SnTiO₃ has a stable *P4mm* phase (with $c/a \approx 1.07$)²². The insertion of the TO-layer (to form SnTi₄O₇) has retained the high tetragonality (i.e. $c/a=1.059$). As the in-plane lattice parameter further increases, the parent SnTiO₃ phase change from the *P4mm* to the *Cm* phase, which is reflected in the decreasing $(c/2)/a$ of SnTi₄O₇ as shown in Fig. 4. Figure 4 also predicts larger room for out-of-plane ion displacements in SnTi₄O₇ than PbTi₄O₇, indicating a larger P_z for the former superlattice (see Sec.III B).

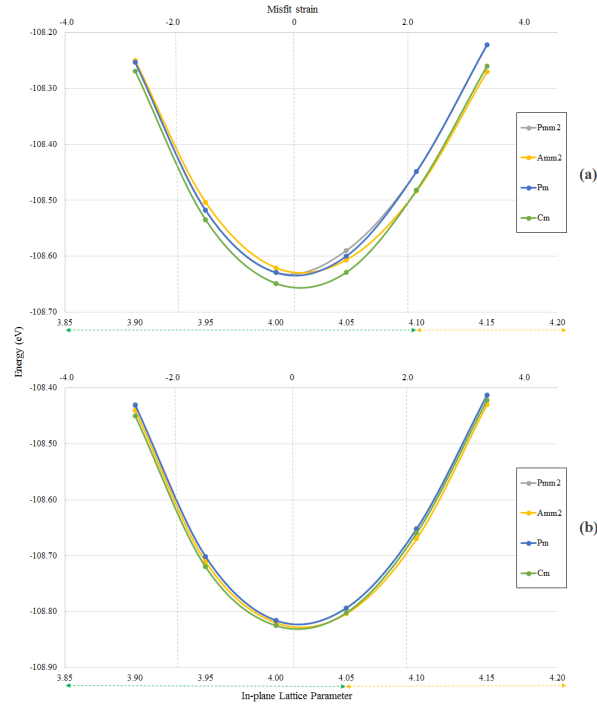


Figure 3. Energy of the epitaxially strained (a) SnTi_4O_7 and (b) PbTi_4O_7 as function of in-plane lattice parameter for $Amm2$, $Pmm2$, Pm , and Cm phase superlattices. Black dotted lines indicate percentage misfit strain on ATi_4O_7 ($A=\text{Sn},\text{Pb}$). Green and yellow dotted lines represent the regions of Cm and $Amm2$ phases.

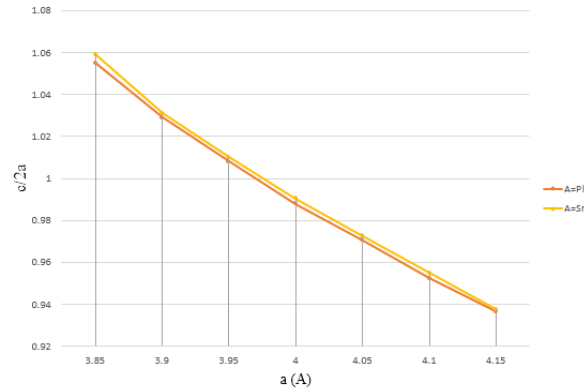


Figure 4. $c/2a$ Ratio as function of in-plane lattice parameter of ATi_4O_7 ($A=\text{Sn},\text{Pb}$)

B. Polarization

Having shown the stability of the various phases of ATi_4O_7 ($A=\text{Sn},\text{Pb}$) superlattice and the effects of epitaxial strain on them, we now proceed to obtain their polarization. Table III compares the spontaneous polarization values of ATiO_3 , A_2TiO_4 ²⁶, and ATi_4O_7 ($A=\text{Sn},\text{Pb}$) in their bulk

Crystal	A=Sn		A=Pb	
	Phase	Polarization	Phase	Polarization
ATiO ₃	<i>P4mm</i>	1.1	<i>P4mm</i>	0.72
A ₂ TiO ₄ (RP)	<i>Aba2</i>	0.53	<i>I2mm</i>	0.68
ATi ₄ O ₇	<i>Cm</i>	0.43	<i>Amm2</i>	0.49

Table III. Comparison of spontaneous polarization (Cm^{-2}) of ATiO₃, A₂TiO₄, and ATi₄O₇(A=Sn,Pb) in their bulk phases^{26,28}.

phases (i.e., not subjected to epitaxial strain), indicating that the proposed structure ATi₄O₇ still possesses a strong polarization despite the added inert TiO layer.

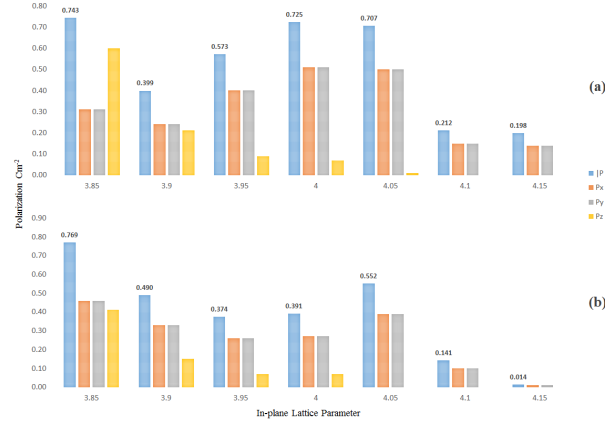


Figure 5. Polarization in single formula unit of (a) SnTi₄O₇ and (b) PbTi₄O₇ with reference to substrate's lattice parameter.

Moreover, it is important to know how polarization is affected by epitaxial strain. Figure 5 shows the polarization of the most stable phases of ATi₄O₇ to facilitate the selection of suitable substrates for their growth. For instance, on the SrTiO₃ substrate (with LDA optimized lattice constant of 3.85\AA ⁹), the corresponding polarization are 0.74 and 0.77 Cm^{-2} for SnTi₄O₇ and PbTi₄O₇, respectively.

Both SnTi₄O₇ and PbTi₄O₇ have similar polarization behavior with respect to external strain. With compressive strain, the *Cm* phase $[(u, u, w)]$ is energetically favorable with a significant P_z due to the strong tendency of out-of-plane ion displacements of the parent perovskite (ATiO₃) in its *P4mm* phase. As the lattice constant expands in the $x - y$ plane, the in-plane polarization ($P_x = P_y$) becomes dominant, eventually resulting in the *Amm2* phase with $P_z = 0$. The overall polarization

decreases significantly as the lattice constant of ATi_4O_7 approaches the initial lattice constant of TiO (i.e. 4.17 \AA), where the displacement of the A ion is suppressed in any direction.

The existence of large P_x and P_y even under a compressive strain is due to the intrinsic nature of ATiO_3 (A=Sn,Pb) which supports in-plane polarization under tensile strain (e.g., the SnTiO_3 part still experiences a tensile strain of 1% when SnTi_4O_7 is under a 2.8% compressive compression). Another important feature of the polarization is the sudden decline in $|P|$ when $a_{\text{ATi}_4\text{O}_7}$ approaches a_{TiO} , which can be explained by the inability of TiO to support polarization due to highly restricted atomic positions with small and strong Ti-O bonds that also hinder the displacements of atoms in the perovskite part (even in the $x-y$ plane). While at smaller in-plane lattice constant, the perovskite part can support polarization, when the lattice constant reaches 4.15 \AA , ATiO_3 is stretched more than 7% while TiO approaches its bulk lattice constant that suppresses polarization.

Moreover, we note that the Cm phase is a rarely occurring phase in pure perovskites (i.e., if the perovskite is not solid solution)^{14,22}. For SnTiO_3 and PbTi_4O_7 , the Cm phase remains up to a tensile strain of 2.15% and 0.95%, respectively, which shows that, the large in-plane lattice mismatch between two crystal structures is a driving force for stabilizing the Cm phase.

C. Superlattice growth

The ATiO_3/TiO superlattice can be fabricated by alternating growth of ATiO_3 and TiO layers using oxide molecular beam epitaxy (O-MBE) or pulsed laser deposition (PLD) methods. With the *in situ* monitoring with reflected high energy electron diffraction (RHEED), the thickness of both ABO_3 and TiO layers, as well as the periodicity, can be precisely controlled. The epitaxial lattice strain can be controlled by properly selecting single crystal perovskite substrates. For instance, the BaTiO_3 (001) and $(1-x)\text{PbMg}_{1/3}\text{Nb}_{2/3}\text{O}_3-x\text{PbTiO}_3$ (PMN-PT) substrates can induce tensile strain while the SrTiO_3 (001), LaAlO_3 (001) substrates can induce compressive strain.

IV. CONCLUSION

Exploiting the large interphase strain driven by combining two crystal structures with high lattice mismatch, we have proposed novel layered structures, i.e., ATi_4O_7 (A=Sn,Pb), and investigated their structural phases, obtaining their basic properties under a wide range of epitaxial strain.

Our first-principles results show a stable Cm phase under strain less than 2.15 and 0.95% for SnTi_4O_7 and PbTi_4O_7 , respectively. We have not investigated the phases involving oxygen octahedron tiltings, therefore, a complete search of possible low-energy phases remains open. However, we have calculated the phonon band structure of the superlattices (see Sec. A), which shows a strong instability at the Γ point, indicating the ground state is most likely a ferroelectric phase.

Our investigation also shows that significant polarization of 0.74 (SnTi_4O_7) and 0.77Cm^{-2} (PbTi_4O_7) can exist if the superlattices are grown on SrTiO_3 substrate. In addition, given the Cm phase, easy polarization rotation is expected in such structures, which can be important for optimizing the shear or longitudinal response in ferroelectrics.

This novel class of materials may serve as an alternative to the formerly investigated Ruddlesden-popper phase to achieve certain desired properties, such as large polarization. With the recent experimental discovery of the giant out-of-plane polarization in PbTiO_3 - PbO thin films owing to a large 16.5% lattice misfit, we believe the insights here will encourage more theoretical and experimental work on them.

Finally, it is important to note that rocksalt TiO is known to be metallic³³⁻³⁵, while ATiO_3 ($A=\text{Sn,Pb}$) is known to be good ferroelectric insulators. Combining them and tuning their ratio may result in a special system with interesting properties.

ACKNOWLEDGMENTS

This work is financially supported by the National Natural Science Foundation of China, Grant No. 11574246, U1537210, and National Basic Research Program of China, Grant No. 2015CB654903. D.W. also thanks the support from the Chinese Scholarship Council (201706285020).

Appendix A: Phonon band structure

To be certain that the procedure we use is correct, we first carry out the ground-state properties investigation of the tetragonal SnTiO_3 and PbTiO_3 crystal structures. A series of calculations were performed to calculate the optimized lattice constants of tetragonal phases of above mentioned perovskite to be compared with values from literature²¹. Table 1 highlights the high similarity of our data with the results from references under consideration; therefore, manifesting for the correctness of our computational parameters.

Property	SnTiO ₃	PbTiO ₃
$a(\text{\AA})$	3.78 (3.78)	3.859 (3.864)
$c(\text{\AA})$	4.28 (4.27)	4.034 (4.051)
$c/a(\text{\AA})$	1.132 (1.129)	1.045 (1.048)
Polarization (Cm ⁻²)	0.99 (1.1)	0.76 (0.72)

Table IV. Optimized structural parameters of tetragonal SnTiO₃ and PbTiO₃ with $P4mm$ symmetry. Comparison is established against the results from reference^{21,22,28,29,31}.

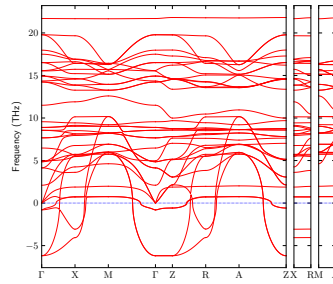


Figure 6. Phonon band structure of ATi₄O₇(A=Pb).

The phonon spectra indicates strong ferroelectric instabilities (FE) at Γ point $\mathbf{k} = (0,0,0)$ whereas the anti-ferroelectric instabilities (AFE) at X (0.5,0,0.5) and anti-ferrodistortive instabilities (AFD) at M(0.5,0,0) and R(0.5,0.5,0.5) are weak. It indicates the possible existence of ferroelectric phases of our SL (as investigated in our work) with negligible affect from AFE and AFD instabilities (which are seen in RP-phase).

* dawei.wang@xjtu.edu.cn

¹ D. G. Schlom et al., MRS Bull. **39**, 118–130 (2014).

² J.-P. et al., Nature **394**, 453–456 (1998).

³ R. von Helmolt, J. Wecker, B. Holzapfel, L. Schultz, K. Samwer, Phys. Rev. Lett. 71, 2331–2333 (1993).

⁴ H. Béa et al., Phys. Rev. Lett. 102, 217603 (2009).

⁵ O. Dieguez and D. Vanderbilt, Phase Transitions, **81**, 607–622 (2008).

⁶ K.M. Rabe, Curr. Opin. Solid St. Matter. Sci. 9, p. 122 (2005).

- ⁷ K.J. Choi, M. Biegalski, Y.L. Li, A. Sharan, J. Schubert, R. Uecker, P. Reiche, Y.B. Chen, X.Q. Pan, V. Gopalan et al., *Science* **306**, 1005 (2004).
- ⁸ J.H. Haeni, P. Irvin, W. Chang, R. Uecker, P. Reiche, Y.L. Li, S. Choudhury, W. Tian, M.E. Hawley, B. Craigo et al., *Nature* **430**, 758 (2004).
- ⁹ R. Zhang, D. Wang, F. Li, H. Ye, X. Wei, and Z. Xu, *Appl. Phys. Lett.* **103**, 062905 (2013).
- ¹⁰ Z. Zhu, *Chinese Phys. B* **27** 027701 (2018).
- ¹¹ Z. Zhen-Ye et al., *Chinese Phys.* **16** 1780 (2007).
- ¹² C.J. Fennie and K.M. Rabe, *Phys. Rev. B* **71**, 100102(R) (2005).
- ¹³ S. N. Ruddlesden and P. Popper, *Acta Crystallogr.* **10**, 538 (1957); **11**, 54 (1958).
- ¹⁴ D. Wang, L.Liu, J. Liu, N. Zhang, and X. Wei, *Epitaxially strained SnTiO₃ at finite temperatures*, *Chin. Phys. B* **27**, 127702 (2018).
- ¹⁵ Z. Jiang, R. Zhang, D. Wang, D. Sichuga, C.L. Jia, and L. Bellaiche, *Phys. Rev. B* **89**, 214113 (2014).
- ¹⁶ M. K. Lee, T. K. Nath, and C. B. Eom, *Applied Physics Letters* Vol. 77, Number 22 (2000).
- ¹⁷ A. H. Larsen et al., *J. Phys.: Condens. Matter* **29** 273002 (2017).
- ¹⁸ J. Enkovaara et al., *J. Phys.: Condens. Matter* **22**, 253202 (2010).
- ¹⁹ Gonze X, Beuken J M, Caracas R, Detraux F, Fuchs M, Rignanese G M, Sindic L, Verstraete M, Zerah G, Jollet F, Torrent M, Roy A, Mikami M, Ghosez P, Raty J Y and Allan D C, *Comput. Mater. Sci.* **25** 478 (2002).
- ²⁰ Y. Uratani , T. Hishidou, and T.O. Guchi, *Jap. J. Appl. Phys.* **47**, 7735 (2008).
- ²¹ Y. B. Xue, D. Chen, Y.J. Wang, Y.L. Tang, Y.L. Zhu & X.L. Ma, *Philosophical Magazine*, **95**:19, 2067-2077, DOI: 10.1080/14786435.2015.1047810 (2015).
- ²² Parker, Rondinelli, and Nakhmanson, *Phys. Rev. B* **84**, 245126 (2011).
- ²³ Zhang et al., *Science* **361**, 494–497 (2018).
- ²⁴ D. Vanderbilt and M. H. Cohen, *Phy. Rev. B* **63**, 094108 (2001).
- ²⁵ J. S. Jang et al., *J. Phys. Chem. C*, pp 15063-15070 (2017).
- ²⁶ Craig J. Fennie and Karin M. Rabe, *Phy. Rev. B* **71**, 100102(R) (2005).
- ²⁷ H. J. Monkhorst, J. D. Pack, *Phys. Rev. B* **13**, 5188 (1976).
- ²⁸ R. Zhang et al., *J. Appl. Phys.* **116**, 174101 (2014).
- ²⁹ S.F. Matar, I. Baraille, and M.A. Subramanian, *Chemical Physics* **355**, 43-49 (2009).
- ³⁰ D. Wang et al., *ACS Omega* **2**, 1036-1039 (2017).
- ³¹ Y. Umeno et al., *Physical Review B* **74**, 060101 (R) (2006).

- ³² G.Saghi-Szabo and R.E. Cohen, Phys. Rev. Lett. **80**, 4321-4324 (1998).
- ³³ S. P. Denker, J. Appl. Phys. **37**, 142 (1965).
- ³⁴ R. Ahuja, O. Eriksson, J. M. Wills, and B. Johansson, Phys. Rev. B **53**, 3072 (1995).
- ³⁵ Y. O. Ciftci, Y. Ünlü, k. Colakoglu, and E. Dielgoz, Phys. Scr. **80**, 025601 (2009).